Metals **2015**, *5*, 1197-1211; doi:10.3390/met5031197

OPEN ACCESS

metals

ISSN 2075-4701

www.mdpi.com/journal/metals/

Article

Thermal Stability of Nanoporous Raney Gold Catalyst

Matthew C. Tai [1], Angus Gentle [1], Kaludewa Sujeewa B. de Silva [1], Matthew D. Arnold [1], Elma van der Lingen [2] and Michael B. Cortie [1,*]

[1] Institute for Nanoscale Technology, University of Technology Sydney, P.O. Box 123, Broadway, NSW 2007, Australia; E-Mails: matthew.c.tai@student.uts.edu.au (M.C.T.); sujeewa.desilva@uts.edu.au (K.S.B.S.); matthew.arnold-1@uts.edu.au (M.D.A.)

[2] Department of Engineering and Technology Management, University of Pretoria, Lynnwood Road, Hatfield, Pretoria 0002, South Africa; E-Mail: elma.vanderlingen@up.ac.za

* Author to whom correspondence should be addressed; E-Mail: michael.cortie@uts.edu.au; Tel.: +61-2-9514-2208.

Academic Editors: Eva Pellicer and Jordi Sort Viñas

Received: 17 June 2015 / Accepted: 1 July 2015 / Published: 7 July 2015

Abstract: Nanoporous "Raney gold" sponge was prepared by de-alloying an Au-Al precursor alloy. Catalytic tests using a micro-reactor confirmed that Raney gold can serve as an active heterogeneous catalyst for CO oxidation, reduction of NO to N_2, and oxidation of NO to NO_2. In general, the specific surface area of a heterogeneous catalyst has an influence on its catalytic efficacy. Unfortunately, gold sponges coarsen readily, leading to sintering of their structure and reduction in surface area. This potentially places constraints on their upper operating temperature in catalytic reactors. Here we analyzed the behavior of Raney gold when the temperature was raised. We examined the kinetics and mechanism of coarsening of the sponge using a combination of *in situ* optical measurements and Metropolis Monte Carlo modeling with a Lennard-Jones interatomic potential. Modeling showed that the sponges started with an isotropic "foamy" morphology with negative average "mean curvature" but that subsequent thermally activated coarsening will drive the morphology through a bi-continuous fibrous state and on, eventually, to a sponge consisting of sintered blobs of predominantly positive "mean curvature".

Keywords: Raney gold; nanoporous gold; catalyst; thermal stability; Monte Carlo

1. Introduction

Nano- or mesoporous gold sponges may be prepared by de-alloying a suitable precursor Au-*X* alloy or intermetallic compound, where *X* is a metallic element that can be selectively dissolved [1]. Forty [2] and Pickering [3] provided early descriptions of these materials, and the term "nanoporous gold" was in use by 1991 [4], if not earlier. There was a significant expansion of interest in these materials after the publication of an influential paper by Erlebacher *et al.* [5] in 2001. A recent book [6] contains an account of some of the newer research. In general, most research on gold sponges has employed Au-Ag precursor alloys (see, for example references [2,4–10]) but other precursors are also feasible. For example, Candy [11] prepared sponge samples in 1981 by de-alloying Au_xAl, and this route has enjoyed some popularity since then, with references [12–16] being a sampling of such work.

The catalytic efficacy of gold nano-sponges was not originally considered however, due probably to the widely held belief prior to the 1990s that gold was not a catalytically active metal [17]. This latter perception slowly changed after the near-simultaneous publication by Haruta [18] and Hutchings [19] that gold nanoparticle heterogeneous catalysts could be exceedingly active under appropriate conditions. Since the mid-1990s there has been considerable scientific and industrial interest in heterogeneous catalysis by very small (<4 nm) gold nanoparticles. Commercial interest in the nanoparticle catalysts has been sustained by their high activity for CO oxidation [20], even at temperatures below 300 K [21], their capability to enhance selective oxidation of propene [22], and their promotion of the water-gas shift reaction at reduced temperatures [23], to cite merely a few technologically-useful examples.

The mechanism of catalysis by gold nanoparticles was believed to involve an electronic interaction between metallic nanoparticle and a suitable oxide substrate, and also appeared to require a quantum-confined band structure in the gold nanoparticle [17,24]. The latter factor placed an upper limit of about 4 nm on the size of catalytic Au nanoparticles (for greater diameters, Au nanoparticles will have electronic properties very similar to those of bulk gold, which is not a catalyst). Since pure, percolated gold nano-sponges have neither the oxide substrate nor the quantum confinement of small nanoparticles, they were not generally thought to be hold any potential as catalysts [20]. However, in 2000, nanoporous gold sponge prepared from Au-Al precursors was found to be a potent catalyst for CO oxidation, NO reduction and NO oxidation. For commercial reasons that work was patented [25] rather than formally published, but aspects of it were publically revealed and discussed at conferences [26–28].

Sponges prepared by de-alloying alloys of the target metal with aluminum are often known as Raney metal sponges in honor of Raney's pioneering work [29] on porous nickel catalysts in 1927; the gold catalysts prepared by this route can be considered to be an example of "Raney gold" and, as such, analogous to other catalysts like "Raney Nickel®" or "Raney copper" [30]. In terms of the IUPAC "gold book" of chemical terminology [31], however, these materials are more correctly described as "mesoporous sponges" since their pore size is in the 2 to 50 nm range. Our "Raney gold"/mesoporous/nanoporous sponge samples were prepared by alkaline de-alloying $AuAl_2$ ("purple gold" [32]) and, when combined with a suitable support, proved to be effective at CO oxidation and both oxidation and reduction of NO [26]. So far, however, they have failed to find a commercial market due to their relatively high gold content and, hence, cost.

Since then, further examples of the catalytic efficacy of nanoporous Au have been reported, mostly in sponges prepared from Au_xAg alloys [33–35]. There have been several subsequent studies of these materials as catalysts for reactions as diverse as CO oxidation [33,35] and oxidative coupling of methanol to methyl formate [36]. In general, however, there is evidence that the catalytic activity in the nanoporous gold produced from (Au, Ag) precursors is correlated with the small quantity of Ag remaining after de-alloying rather than to the gold on its own [36–38]. In the present paper we concentrate on the properties of Raney gold rather than the sponge produced from (Au, Ag). In this case, confusion from any possible role of Ag does not arise. Actually, Raney gold may have applications beyond catalysis and, for example, has been studied for use in applications requiring spectrally-selective coatings [3], capacitive biosensors [4], or even as the basis of an ultra-efficient supercapacitor [5].

2. Experimental Section

2.1. Manufacture of Raney Gold Catalyst Powders and Thin Films

Samples of $AuAl_x$, where $x \approx 2$, were produced by vacuum-arc melting (bulk samples) or by magnetron sputtering (thin-film samples). In some cases alloying element additions were made to the precursor; for example, the effect of Fe was tested by making a 5 wt % Fe addition to the $AuAl_x$ melt. The bulk samples were then dry milled to powder using a Sieb mill (Siebtechnik GmbH, Mülheim an der Ruhr, Germany), followed by further reduction in alcohol in a "micronizing" mill. Powders were either milled as-is, or together with a catalytic support, such as hopcalite (a 3:1 mixture of MnO_2 and CuO) or Co_3O_4. After milling, the powders were sized by sieving and the 2 to 5 μm fraction used.

Catalytic efficacy was tested courtesy of former colleagues at Project Autek of Mintek (see Acknowledgements). A fixed-bed, stainless steel micro-reactor equipped with a temperature-controlled reaction chamber was loaded with 0.5 g catalyst at a time. Oxidation of CO was tested in a gas stream of 1% CO in air. In the case of the Raney gold/hopcalite catalyst the gas was flowed through the micro-reactor at a space velocity (SV) of 9 $L \cdot g^{-1}cat \cdot h^{-1}$. Two comparators were also tested: standard hopcalite and hopcalite on which Au nanoparticles had been precipitated by aqueous "deposition-precipitation". In the case of Raney gold sponge, with and without Fe additions, SV's 18 and 36 $L \cdot g^{-1}cat \cdot h^{-1}$ were used, due to the higher activity of these catalysts. Gas composition was controlled by mass flow controllers while reaction products were analyzed by a Shimadzu 17A gas chromatograph (Shimadzu Corporation, Kyoto, Japan).

The effect of the de-alloying conditions was also assessed. For powder produced from the bulk samples, NaOH with concentrations of between 0.5 and 2 M is suitable, but the most active catalysts were obtained with 1 M NaOH, temperatures below 8 °C, and de-alloying times of the order of a day. Under these circumstances less than 5 at. % Al remained in the catalyst. However, even better activity and durability was obtained by milling the $AuAl_2$ precursor together with a transition metal oxide like Co_3O_4 before de-alloying, or alternatively adding promoting elements such as Fe into the $AuAl_2$ precursor when it was first melted.

Thin film samples were de-alloyed with 0.1 or 0.2 M NaOH for about 1 to 4 min. They were quite fragile and de-alloying for too long led to the samples floating off their glass substrates. The Al

contents of the precursor Au-Al films were in the range of 65 to 75 at.%. After the three minutes of de-alloying, the Al contents of these samples were in the range of 15 ± 5 at.% Al. Thin films produced by deposition at ~300 °C had a very much rougher surface than those deposited at room temperature due to the growth of $AuAl_2$ crystals on the surface. They also de-alloyed more rapidly, probably due to their greater surface area.

2.2. Modelling of Coarsening Using Metropolis Monte Carlo Method

The de-alloying process and subsequent coarsening of the sponge were modelled by an off-lattice Metropolis Monte Carlo code. Some background information on the code is available elsewhere [39]. Briefly, the problem of determining atom neighbors in an off-lattice simulation was solved by hashing atomic positions to a large 3D integer hash array. De-alloying was achieved using a stochastic cellular automaton [40] that, in this case, randomly removed surface Al atoms. Relaxation of the structure was achieved using a Lennard-Jones (LJ) potential. The LJ 12-6 potential was used with a cut off at 2.5 LJ length units. (It is convenient to use a dimensionless system of units in these simulations. In LJ units, the distance at which the interatomic potential is most negative is 1.0 LJ length units and the depth of the energy well is 1.0 LJ energy units. Temperature is measured in energy units and, for example, melting of a face-centered cubic lattice occurs at $T \approx 0.75$. Time is measured in "sweeps", where one sweep has elapsed when, on average, each atom in the simulation has been selected once by the Monte Carlo loop.) The precursor crystals were face-centered cubic with 100,000 randomly distributed Al and Au atoms, placed on an inert, horizontal substrate. The simulation volume corresponded approximately to a 8.7 × 6.3 × 6.3 nm cuboid. Periodic boundary conditions were imposed in the plane of the substrate but the lower and upper bounds of the simulation in the vertical direction were made to be impermeable. The simulations were run a high performance computing cluster or on a high performance desktop. The program was written for FPC (Free Pascal Compiler) which compiles to fast native code on Linux, Windows or Mac systems.

Curvature of the resulting sponges was determined by an algorithm that identified surface atoms, and which then fitted biquadratic surface patches centered on selected surface atoms. Average "mean curvature", <M> in units of LJ length^{-1}, and average "Gaussian curvature", <G> in units of LJ length^{-2}, were obtained from 5000 randomly selected patches per sponge. An individual negative mean curvature implies a hole or concavity in the solid, a positive mean curvature corresponds to a solid sphere or convex protrusion. An individual negative Gaussian curvature implies that the surface has a saddle point in the vicinity of the chosen surface atom. A positive Gaussian curvature could correspond to either a solid sphere or a hole. Use of the <M> or <G> provided an indication of the sponge's average morphology.

2.3. Analysis of Coarsening Using in Situ Optical Measurements

Samples of Raney gold sponge were subjected to coarsening heat treatments while their optical properties were monitored *in situ*. Large changes in the morphology of the sponge during heating experiments were readily detected by changes in the reflectance of the sample, determined using an Ocean Optics USB 2000 (340–1020 nm) spectrometer (Ocean Optics, Dunedin, FL, USA) and a tungsten halogen light source, at an angle of about 30° off vertical. The sponges gradually develop a

yellow color on heating, which is detectable by eye once coarsening has proceeded sufficiently. The more subtle changes in the sponge morphology that preceded the development of the yellow color were followed by measuring the amplitude ratio ψ between incoming and outgoing polarized radiation using a V-VASE Ellipsometer (J.A. Woollam Co., Lincoln, NE, USA) In this case the sample was ramped at 10 °C·min^{-1} to a series of set-point temperatures. Optical measurements were taken with a one minute dwell time at each temperature, up to 100 °C. The sample was then held at 100 °C for all further measurements. The changes in reflectance and ψ were used merely as indicators that some kind of geometric change was occurring in the sponge, and we did not attempt to obtain a quantitative relationship between the optical proxies and actual geometric changes in morphology of the sponge. The coarsening experiments were performed in air. Scanning electron microscope images of the sponges were taken using "in lens" mode on a Zeiss Supra 55 VP (Zeiss, Oberkochen, Germany).

3. Results and Discussion

3.1. Morphology of Nanoporous Raney Gold Sponge

In our work, de-alloying of homogeneous $AuAl_x$ precursors produced sponge types varying from "pinhole" to isotropic foamy to skeletal (see Figure 1). Foamy sponges consist of interconnected spherical pores within a solid matrix. This is marked contrast to the sponges produced by de-alloying Au-Ag alloys, which are isotropic fibrous sponges consisting of a classic bi-continuous network of interpenetrating channels and ligaments [1,2,4–10]. Fibrous sponges have also been produced from Au-Al precursors by other workers [15], however, so the controlling factor is clearly not just the precursor composition and clearly also involves the manner in which de-alloying was performed. Certainly, it is known that the nature of the de-alloying solution has a major effect on the surface diffusivity of the Au atoms [1] and we believe that foam sponges are favored by the use of dilute NaOH. In prior work we have been able to produce both kinds of sponge from the same composition range of Pt_xAl precursors [39]. The two kinds of sponge—foamy and fibrous—are correlated with quite different mathematical characteristics; the former is characterized by an average "mean curvature" that is negative but an average "Gaussian curvature" that is positive, whereas the fibrous type of sponge has a positive average mean curvature and, on average, a Gaussian curvature that straddles zero [39].

Raney gold produced from bulk material contains about 5 at.% residual Al after 40 h of de-alloying in 1 M NaOH. In contrast, sponges produced by de-alloying thin films for 3 min in 0.1 or 0.2 M NaOH contain of the order of 15 at.% Al. Either way, the ligaments of these sponges are between 3 and 11 nm thick (high resolution SEM) with a pore diameter in the 5 to 20 nm range. This is in good agreement with a previously reported [27] average crystallite size of 7 nm (found from the Scherrer equation and X-ray diffraction) and an average pore size of 12 ± 5 nm [12]. Note that, if desired, the material can be prepared to have a bimodal distribution of pores clustered around the 10 nm and 30 nm sizes [41] by arranging for the precursor to contain a dual-phase microstructure. Freshly de-alloyed Raney gold produced from the bulk samples has a BET surface area of the order of 20 m^2·g^{-1}. This is about double the BET surface area reported[1] for the nanoporous sponge produced by de-alloying Au_xAg.

It was also noticed that magnetron deposition onto a high-temperature substrate produces a precursor with a very rough surface, due to the formation of crystals of $AuAl_2$ that grow out of the plane. Similar phenomena occur in the Pt-Al system [39]. When these protruding crystals are de-alloyed, a bimodal morphology is produced, with the crystals generating a different type of sponge to the underlying material (see Section 3.3). This strategy provides an additional way to tune the sponge morphology and increase its surface area.

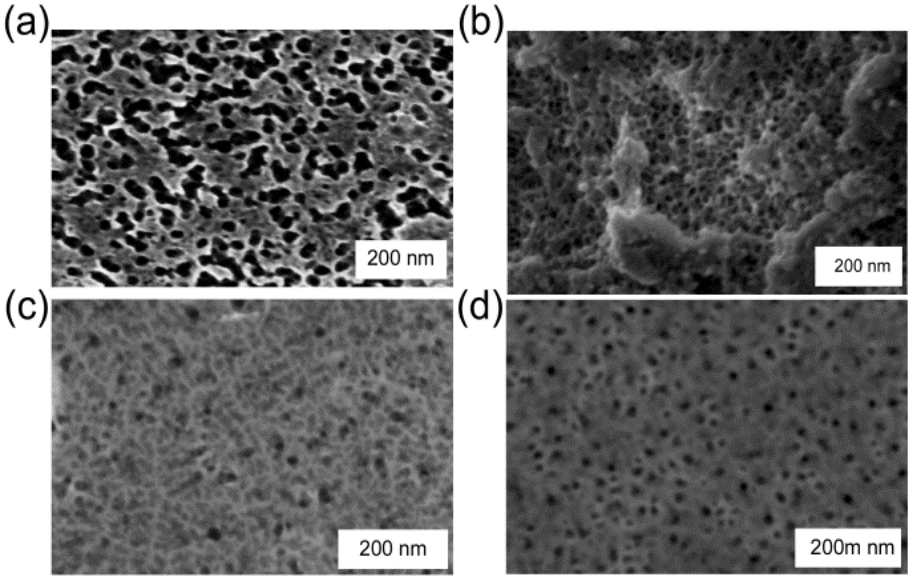

Figure 1. Scanning electron microscope images of nanoporous sponges prepared in Au by de-alloying $AuAl_2$, (**a**) thin film showing irregularly-shaped ligaments and pores (image courtesy of Dr. A Maaroof, 0.2 M NaOH, ~3 min); (**b**) de-alloyed bulk $AuAl_2$ showing foamy sponge (0.1 M NaOH, room temperature, 30 min); (**c**) sponge with skeletal morphology produced from a 72 at.% Al precursor (0.1 M NaOH, 2 min); (**d**) "pinhole"-type sponge produced from a 66 at.% Al precursor (0.1 M NaOH, 4 min).

3.2. Catalysis by Raney Gold

The catalytic efficacy of these materials varied widely. Some prior information on our Raney gold catalysts was made available in conference talks and patents [25–28].

Oxidation of CO was initially rapid for both the standard hopcalite comparator and for the two gold catalysts tested (gold nanoparticles on hopcalite, and gold sponge mechanically mixed with hopcalite). At 60 °C, conversion for all three types was initially about 90%. The activity of Au-free hopcalite decreased over time, a well-known phenomenon [42] that is apparently due to poisoning by H_2O. After 10 h, the pure hopcalite catalyst could only convert 50% of the CO. A hopcalite/gold nanoparticle catalyst prepared by deposition-precipitation fared better and was still converting 70% of the CO after 10 h. In contrast, the hopcalite/gold sponge catalyst delivered outstanding performance, retaining its 90% conversion rate for the 18 h of the experiment. Conversion at 20 h was improved from 85% to 98% by increasing the loading of the Raney gold on the hopcalite from 1 wt % to 5 wt %, however, the increased cost of the higher gold loading would make this a doubtful proposition in a commercial application.

Since hopcalite is already a catalyst for CO conversion, the role of the Au is merely to improve an existing functionality further. Therefore, nanoporous gold sponges were also tested in the absence of hopcalite (see Figure 2). Performance of a pure gold sponge was relatively poor under these conditions, but that of a $AuAl_2$ + 5 at.% Fe precursor was markedly better. Even better performance was obtained by pre-oxidizing the Fe in the $AuAl_2$/Fe precursor alloy powder for ~12 h in air at 200 °C, prior to de-alloying. This sample was so active that it had to be tested at twice the space velocity of the other two, yet it still produced much better conversion efficiencies. XPS analysis of this very active sample indicated that, in addition to Au $4f_{7/2}$ and Au $4f_{5/2}$ peaks due to Au at 84.1 ± 0.1 eV and 87.7 ± 0.1 eV, additional peaks appeared at 86.4 ± 0.1 eV and 89.9 ± 0.1 eV after 23 h of testing in the 1% CO/air mixture. These new peaks correspond to those of Au_2O_3 [43], which evidently formed while the catalyst was on stream. This is an unexpected finding. The XPS also indicated that most Fe was likely present as Fe^{3+}, which is as expected.

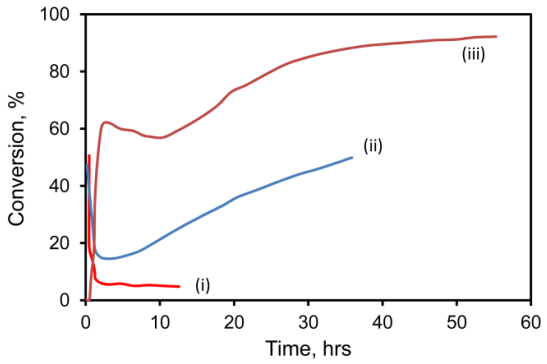

Figure 2. Conversion of 1% CO—air mixture over (**i**) pure mesoporous Au at 60 °C; (**ii**) mesoporous Au/Fe at 60 °C and (**iii**) mesoporous Au/Fe at 60 °C after 12 h of oxidation at 200 °C (space velocity at 60 °C was 18 $L \cdot g^{-1} \cdot h^{-1}$ for curves (**i**) and (**ii**), and 36 $L \cdot g^{-1} \cdot h^{-1}$ for curve (**iii**)) (data courtesy of Project AuTEK, Mintek, South Africa).

The excellent performance of Fe-doped Raney gold catalysts for CO oxidation presumably arises from similar factors to those that make Au/Fe_2O_3 catalysts so active [20,43] for this reaction. Specifically, the mechanism of catalysis hypothesized [20] by Bond and Thompson holds that catalysis in Au^0/M_xO_y systems requires [21] a perimeter region of $Au^{\delta+}$ species to act as a bridge between the Au^0 and the M_xO_y support. In this respect, the probable presence of Au_2O_3 on the surface of the most active of the three Raney gold samples above is supportive of the hypothesis. Note, in contrast, that the mechanism proposed earlier by Haruta [21,38] requires only that Au^0 be bound at an atomic level to the M_xO_y.

The conversion efficiency of these catalysts showed a complicated behavior with time. We will return to this point later.

The catalytic conversion data for CO show two opposing effects. First, there is a very rapid fall off in efficacy with time at 60 °C and indeed, in some trials, efficacy begins at zero. Opposing this fall off is a time-dependent increase in conversion in the catalysts containing Fe. We suggest that the initial fall off in conversion efficiency is due to the coarsening of the nanoporous gold sponge, even at temperatures below 100 °C. The coarsening removes asperities in the sponge and causes a decrease in specific surface area with time. Coarsening in Au sponges is abetted by the relatively high surface

tension [44] of metallic gold and has been recognized as a problem in these materials [45]. It is possible that it could be retarded by alloying with a third element such as Pt [45] or by deliberate generation of a refractory surface oxide like Al_2O_3 [41]. In the present instance, however, the purely physical effect of coarsening is opposed by some chemical phenomenon involving Fe, in terms of which activity increases over time. We suspect that this may involve the development of domains of catalytically-active nanoporous Fe_xO on the catalyst surface but further work is required to verify this.

3.3. Coarsening of Raney Gold Sponges

Information on the coarsening behavior of Raney gold sponge was acquired using optical measurements applied to a range of thin film samples. First, we exploited the color change that occurred on coarsening. Freshly de-alloyed Raney gold has a very flat spectral response in the visible part of the spectrum [46], and is basically "black". However, as it coarsens, the reflectance at longer wavelengths rises, while that at shorter wavelengths decreases. In the limit, these trends would give the ~550 nm absorption edge and famous yellow color of bulk gold. The change can be captured as the difference in reflectance between that at 660 nm and that at 520 nm. In Figure 3 we show this parameter for a thin film of Raney gold ramped at 6 °C·min^{-1}. It is clear that significant changes occurred in the morphology of the sponge as the temperature rose above 100 °C and that it had acquired an absorption edge by about 250 °C.

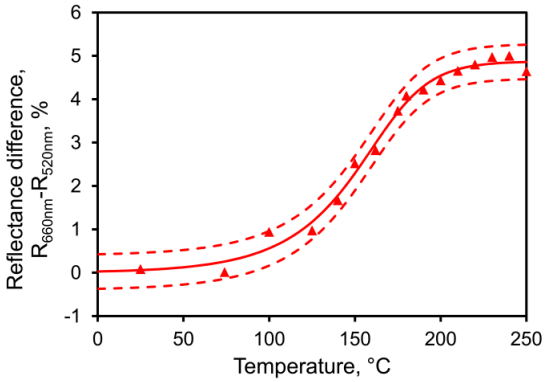

Figure 3. Development of an optical absorption edge in a thin film of gold sponge determined *in situ* while ramped at 6 °C·min^{-1}. The sponge coarsens quite rapidly above 100 °C. A sigmoidal model (Richard's model, solid line) and 95% confidence interval (dashed lines) have been fitted to guide the eye. Sample deposited as 76 at.% Al and de-alloyed in 0.2 M NaOH.

A more sensitive indication of the change in sponge morphology can be obtained by using the ψ value from ellipsometric measurements which is sensitive to the optical properties of the sponge. In the present context this parameter can be considered to be merely an indirect proxy for morphological changes in the sponge: a change in ψ is indicative of a change in the effective refractive of the sponge and, hence, of its structure. The variation of ψ with temperature is shown in Figure 4a. (The precursor for this particular sponge was deposited with ~66 at.% Al at ~300 °C and is an example of a sponge with a "rough" surface, as discussed in Section 3.1.) It is clear that, for these conditions, the morphology of sponge starts to change noticeably at about 35 °C. As the temperature is increased, the

rate of change is greater. The rate of change in ψ (dψ/d*T*) is quite rapid above 75 °C and continues during an isothermal anneal at 100 °C (see Figure 4b). The coarsening process in gold relies upon surface diffusion of the gold atoms and, like other diffusive processes, is thermally activated [1]. This means that the probability of a diffusive event occurring rises exponentially with an increase in temperature. Diffusion in gold is negligible at room temperature or below, but will be accelerated markedly as the temperature rises above room temperature. In our case the rate is clearly already quite appreciable at 100 °C. Figure 5 shows a series of SEM images, taken on samples annealed at increasingly higher temperatures in the experiment depicted in Figure 4.

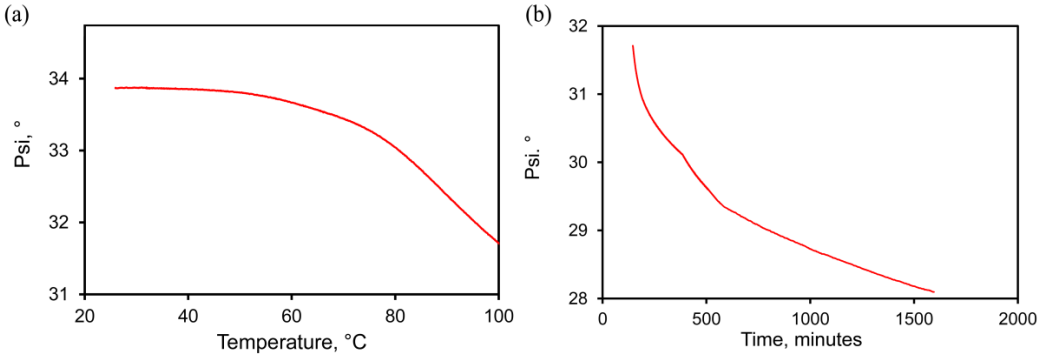

Figure 4. Change in optical ψ value of sample as a proxy for its density, determined during *in situ* heating in an ellipsometer. Sample was deposited at ~300 °C with ~65% Al and was de-alloyed in 0.1 M NaOH for 2 min. (**a**) During ramp to 100 °C; (**b**) During isothermal heat treatment at 100 °C.

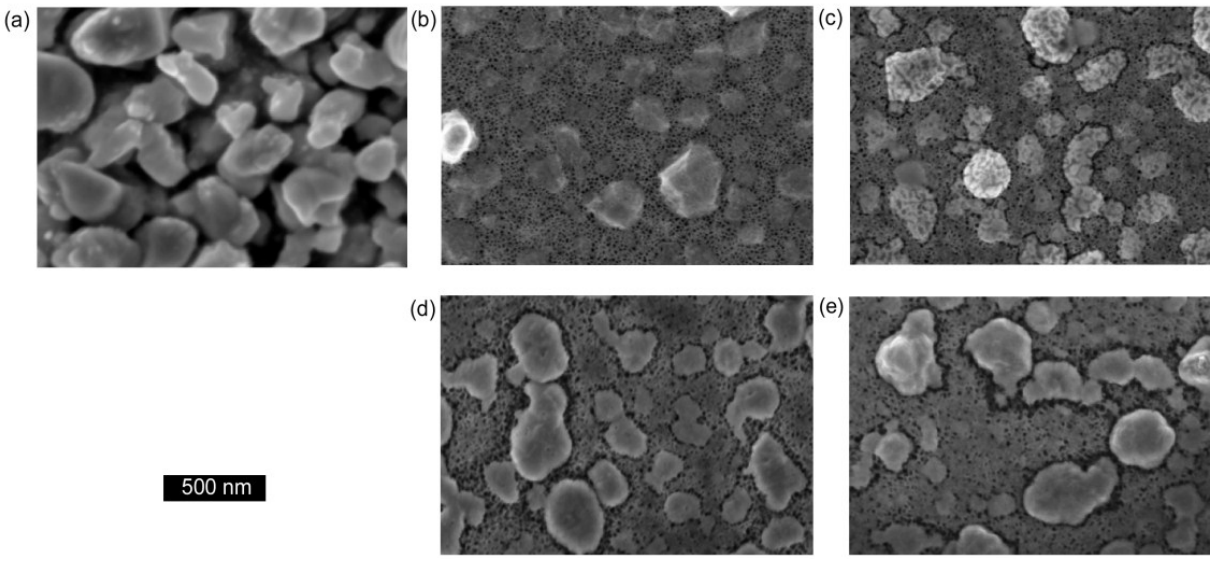

Figure 5. Scanning electron microscope images of nanoporous showing the change in morphology of sponge as a function of annealing temperature, (**a**) as-deposited at ≈300 °C; (**b**) immediately after de-alloying; (**c**) after heating to 50 °C; (**d**) after heating to 100 °C; (**e**) after heating to 330 °C (0.1 M NaOH, de-alloyed for 1 min).

3.4. Metropolis Monte Carlo Modelling of Sponge Coarsening

The Monte Carlo calculations were successful at simulating both de-alloying and coarsening. A series of cut-away views of a nanoporous sponge produced from a precursor containing 65 at.% Al is shown in Figure 6. It can be seen that de-alloying at $T = 0.18$ begins with widespread pitting attack on the exposed surface, with the pits rapidly penetrating below the surface. In a relatively short time the sponge is comprised of interpenetrating ligaments and cavities through to its inert substrate. The sponge then slowly coarsened when it was subsequently annealed at $T = 0.4$. The ratio of surface atoms to total number of atoms (which is a proxy for specific surface area) decreased, in all of the sponges, at a rate that was dependent on both time and temperature (see Figure 7a). Associated with this coarsening was a change in the morphology of the sponges. In Figure 7b, we plot the proportion of surface patches with negative Gaussian curvature (which indicate saddle points) against the proportion of surface patches with positive mean curvature (which indicate generally convex features, including saddle points in which positive mean curvature dominates). It is clear that the model sponges produced from precursors with between 60 and 85 at.% Al all started off as foams, with an abundance of percolating holes, tunnels, and cavities of overall negative mean curvature. However, as the coarsening proceeded, the sponges reorganized. Those produced from the precursors of 60% to 75% Al rearranged into the classic bi-vermicular fibrous sponge morphology which has an abundance of saddle points and an overall positive mean curvature. In contrast, the sponges produced by de-alloying the 80 and 85 at.% Al precursors, however, were not dense enough to stabilize the fibrous structure and the solid material within them collapsed into approximately spherical blobs, to produce a granular sponge. In the case of the model sponge produced from the 85 at.% Al precursor it is clear that, if annealing is carried on long enough, the structure will eventually lose percolation as it morphs into an ensemble of spherical blobs (see Figure 8). Experimental evidence for such de-percolated sponges has been found for the case Pt sponge [39] and this places an upper limit on how much Al may be in the precursor if a reasonably percolated and mechanical robust sponge is desired.

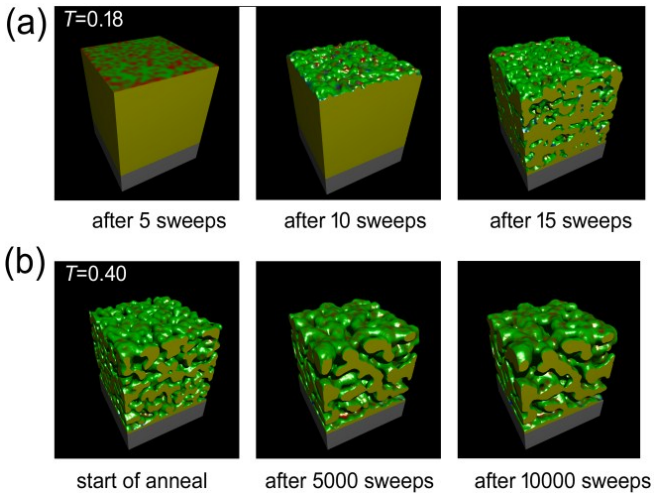

Figure 6. Results of Monte Carlo simulation of the evolution of sponge morphology with time for the case of a sponge prepared from precursor containing 65 at.% Al. (**a**) Change in morphology at $T = 0.18$ as de-alloying proceeds, (**b**) Change in morphology at $T = 0.40$ as sponge is annealed.

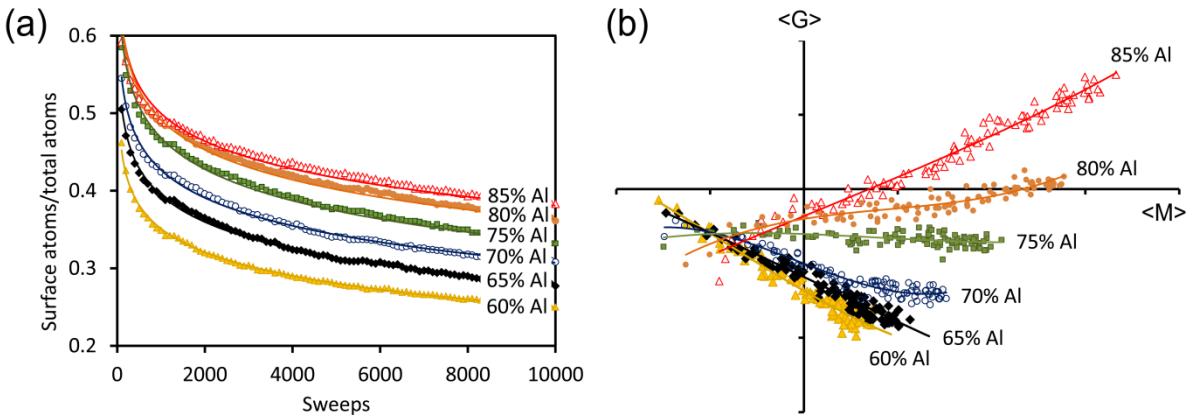

Figure 7. Changes in morphology in model sponges prepared from precursors containing between 60 and 85 at.% Al, as a function of Monte Carlo annealing time at $T = 0$. (**a**) ratio of surface atoms to total atoms; (**b**) average Gaussian curvature (<G>) plotted against average "mean curvature" (<M>) for the sponges shown in (**a**). Simulations start in the bottom left quadrant and sponge evolve towards more positive values of <M>.

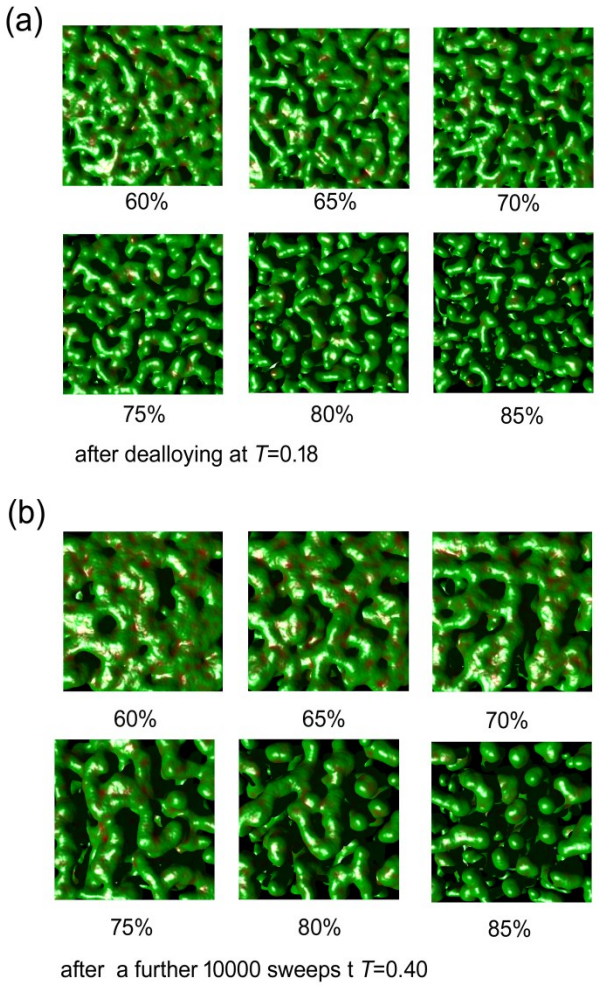

Figure 8. Effect of 10,000 Monte Carlo annealing sweeps at $T = 0.4$ on the morphology of model de-alloyed sponges prepared using series of precursors containing from 60 to 85 at.% Al (top view).

4. Conclusions

The catalytic capabilities of mesoporous/nanoporous gold have been known since 2001. The early work focused on the properties of "Raney gold"-type materials produced by de-alloying $AuAl_x$. The compound $AuAl_2$, also known as "purple gold" is an example of a suitable precursor. Raney gold is active for CO and NO oxidation, and NO reduction, however, optimization of the catalytic efficacy usually requires the presence of transition metal oxides in or on the nanoporous sponge. Fe_xO, Co_xO and hopcalite (Mn_xO/Cu_xO mixture) are examples of suitable metal oxides for enhancing the basic Raney gold catalyst. It is possible that the residual Al content of the plain sponge is oxidized and that the presence of this may contribute to the catalysis.

Like other heterogeneous catalysts, the activity of Raney gold depends on its specific surface area—the greater the available surface then the more sites available on which the chemical reaction can be catalyzed. Unfortunately, nanoporous gold sponges, including Raney gold sponge, are thermally unstable. The relatively high surface tension of Au in combination with its oxide-free surface and a high surface diffusion coefficient cause these sponges to undergo thermally-activated coarsening. The result is a coarsening of the microstructure and a reduction in specific surface area. The clear implication is that Raney gold catalyst is susceptible to loss of catalytic efficacy due to coarsening, a thermally-activated process driven by time and temperature. However, the detrimental effects of loss of surface area can be offset by chemical changes to the catalyst surface. For example, in the present case it appears that changes to the Fe_xO on the surface of sponge strongly promote conversion of CO as time elapses. It could be very worthwhile to identify what these critical factors are.

The coarsening phenomenon can be followed using changes in the optical properties of the sponge as a proxy for changes in morphology. Coarsening is detectable at temperatures as low as 35 °C and is already quite significant at 100 °C. Monte Carlo simulations provide a suggested pathway for the evolution of specific surface area and sponge morphology with time and temperature. These simulations predict that the average "mean curvature" of sponges produced from precursors containing between 65 and 85 at.% Al will start off as negative (*i.e.*, foamy), but will transition to positive as a fibrous bi-continuous morphology develops during coarsening. The ratio of surface to total atoms will decrease with time in all three types of sponge, particularly as the temperature is raised.

Acknowledgments

The measurements of catalytic activity were obtained by G. Pattrick and his colleagues at Project AuTEK, Advanced Materials Division, Mintek, South Africa. We thank the Australian Research Council for financial support.

Author Contributions

Fabrication of thin films and optical characterization—Matthew Tai, Angus Gentle, Kaludewa Sujeewa de Silva. Monte Carlo simulations—Matthew Tai, Michael B. Cortie and Matthew Arnold. Catalyst and XPS data—Elma van der Lingen.

Conflicts of Interest

The authors declare no conflict of interest.

References

1. Qiu, H.-J.; Peng, L.; Li, X.; Xu, H.T.; Wang, Y. Using corrosion to fabricate various nanoporous metal structures. *Corros. Sci.* **2015**, *92*, 16–31.
2. Forty, A.J. Corrosion micromorphology of noble metal alloys and depletion gilding. *Nature* **1979**, *282*, 597–598.
3. Pickering, H.W.; Kim, Y.S. De-alloying at elevated temperatures and at 298K—Similarities and differences. *Corros. Sci.* **1982**, *22*, 621–635.
4. Kelly, R.G.; Frost, A.J.; Shahrabi, T.; Newman, R.C. Brittle-fracture of an Au/Ag alloy induced by a surface-film. *Metall. Trans. A* **1991**, *22*, 531–541.
5. Erlebacher, J.; Aziz, M.J.; Karma, A.; Dimitrov, N.; Sieradzki, K. Evolution of nanoporosity in dealloying. *Nature* **2001**, *410*, 450–435.
6. Wittstock, A.; Biener, J.; Erlebacher, J.; Bäumer, M. *Nanoporous Gold: From an Ancient Technology to a High.-tech Material*; Royal Society of Chemistry Publishing: Cambridge, UK, 2012.
7. Ding, Y.; Erlebacher, J. Nanoporous metals with controlled multimodal pore size distribution. *J. Am. Chem. Soc.* **2003**, *125*, 7772–7773.
8. Erlebacher, J. An atomistic description of dealloying—Porosity evolution, the critical potential, and rate-limiting behavior. *J. Electrochem. Soc.* **2004**, *151*, C614–C626.
9. Fujita, T.; Qian, L.-H.; Inoke, K.; Erlebacher, J.; Chen, M.-W. Three-dimensional morphology of nanoporous gold. *Appl. Phys. Lett.* **2008**, *92*, 251902.
10. Parida, S.; Kramer, D.; Volkert, C.A.; Rösner, H.; Erlebacher, J.; Weissmüller, J. Volume change during the formation of nanoporous gold by dealloying. *Phys. Rev. Lett.* **2006**, *97*, 035504.
11. Candy, J.P.; Fouilloux, P.; Keddam, M.; Takenouti, H. The characterization of porous electrodes by impedance measurements. *Electrochim. Acta* **1981**, *26*, 1029–1034.
12. Cortie, M.B.; Maaroof, A.; Smith, G.B.; Ngoepe, P. Nanoscale coatings of $AuAl_x$ and $PtAl_x$ and their mesoporous elemental derivatives. *Curr. Appl. Phys.* **2006**, *6*, 440–443.
13. Cortie, M.B.; Maaroof, A.I.; Smith, G.B. Electrochemical capacitance of mesoporous gold. *Gold Bull.* **2005**, *38*, 15–23.
14. Zhang, Z.; Wang, Y.; Qi, Z.; Somsen, C.; Wang, X.; Zhao, C. Fabrication and characterization of nanoporous gold composites through chemical dealloying of two phase Al–Au alloys. *J. Mater. Chem.* **2009**, *19*, 6042–6050.
15. Zhang, Z.; Wang, Y.; Wang, Y.; Wang, X.; Qi, Z.; Jia, H.; Zhao, C. Formation of ultrafine nanoporous gold related to surface diffusion of gold adatoms during dealloying of Al_2Au in an alkaline solution. *Scr. Mater.* **2010**, *62*, 137–140.
16. Wang, X.; Zhang, Z.; Ji, H.; Xu, J.; Huang, X.; Ma, Y. Dealloying of single-phase Al_2Au to nanoporous gold ribbon/film with tunable morphology in inorganic and organic acidic media. *Appl. Surf. Sci.* **2012**, *258*, 9073–9079.

17. Bond, G.C. Gold: A relatively new catalyst. *Gold Bull.* **2001**, *34*, 117–119.
18. Haruta, M.; Kobayashi, T.; Sano, H.; Yamada, N. Novel gold catalysts for the oxidation of carbon-monoxide at a temperature far below 0 °C. *Chem. Lett.* **1987**, *4*, 405–408.
19. Hutchings, G.J. Vapor-phase hydrochlorination of acetylene—Correlation of catalytic activity of supported metal chloride catalysts. *J. Catal.* **1985**, *96*, 292–295.
20. Bond, G.C.; Thompson, D.T. Gold-catalysed oxidation of carbon monoxide. *Gold Bull.* **2000**, *33*, 41–51.
21. Haruta, M. Gold as a novel catalyst in the 21st Century: Preparation, working mechanism and applications. *Gold Bull.* **2004**, *37*, 27–36.
22. Hayashi, T.; Tanaka, K.; Haruta, M. Selective vapor-phase epoxidation of propylene over Au/TiO_2 catalysts in the presence of oxygen and hydrogen. *J. Catal.* **1998**, *178*, 566–575.
23. Andreeva, D. Low temperature water gas shift over gold catalysts. *Gold Bull.* **2002**, *35*, 82–88.
24. Bond, G.C.; Thompson, D.T. Catalysis by gold. *Catal. Rev. Sci. Eng.* **1999**, *41*, 319–388.
25. Glaner, L.; van der Lingen, E.; Cortie, M.B. Gold Catalysts and Methods for Their Preparation. Australian Patent 2003/215039, 30 January 2003.
26. Cortie, M.B.; van der Lingen, E.; Pattrick, G. Catalysis and capacitance on nano-structured gold particles and sponges. In Proceedings of the Asia Pacific Nanotechnology Forum 2003, Cairns, Australia, 19–21 November 2003; World Scientific: Singapore, 2003.
27. Van der Lingen, E.; Cortie, M.B.; Schwarzer, H.; Roberts, S.J.; Pattrick, G.; Compton, D. Gold catalysts prepared via intermetallic precursor. In Proceedings of the Gold 2003: New Industrial Applications for Gold, Vancouver, Canada, 28 September–1 October 2003;World Gold Council and Canadian Institute of Mining, Metallurgy and Petroleum: London, UK and Westmount, QC, Canada, 2003.
28. Pattrick, G.; van der Lingen, E.; Schwarzer, H.; Roberts, S.J. Development of gold-sponge catalysts for lean-burn $deNO_x$. In Proceedings of the Gold 2003: New Industrial Applications for Gold, Vancouver, Canada, 28 September–1 October 2003;World Gold Council and Canadian Institute of Mining, Metallurgy and Petroleum: London, UK and Westmount, QC, Canada, 2003.
29. Raney, R.M. Method of Producing Finely-Divided Nickel. US Patent 1628190, 10 May 1927.
30. Tomsett, A.D.; Young, D.J.; Wainwright, M.S. Modelling the development of pore structure during the preparation of Raney copper catalysts for fixed bed operation. *Appl. Catal.* **1987**, *35*, 321–328.
31. McNaught, A.D.; Wilkinson, A. *Compendium of Chemical Terminology*; Blackwell Scientific Publications: Oxford, UK, 1997.
32. Supansomboon, S.; Maaroof, A.; Cortie, M.B. "Purple glory": The optical properties and technology of $AuAl_2$ coatings. *Gold Bull.* **2008**, *41*, 296–304.
33. Jürgens, B.; Kübel, C.; Schulz, C.; Nowitzki, T.; Zielasek, V.; Biener, J.; Biener, M.M.; Hamza, A.V.; Bäumer, M. New gold and silver-gold catalysts in the shape of sponges and sieves. *Gold Bull.* **2007**, *40*, 142–149.
34. Zielasek, V.; Jürgens, B.; Schulz, C.; Biener, J.; Biener, M.M.; Hamza, A.V.; Bäume, M. Gold catalysts: Nanoporous gold foams. *Angew. Chem. Int. Ed.* **2006**, *45*, 8241–8244.
35. Xu, C.; Su, J.; Xu, X.; Liu, P.; Zhao, H.; Tian, F.; Ding, Y. Low temperature CO oxidation over unsupported nanoporous gold. *J. Am. Chem. Soc.* **2007**, *129*, 42–43.

36. Wittstock, A.; Zielasek, V.; Biener, J.; Friend, C.M.; Bäumer, M. Nanoporous gold catalysts for selective gas-phase oxidative coupling of methanol at low temperature. *Science* **2010**, *327*, 319–322.
37. Iizuka, Y.; Kawamoto, A.; Akita, K.; Date, M.; Tsubota, S.; Okumura, M.; Haruta, M. Effect of impurity and pretreatment conditions on the catalytic activity of Au powder for CO oxidation. *Catal. Lett.* **2004**, *97*, 203–208.
38. Haruta, M. Chance and necessity: My encounter with gold catalysts. *Angew. Chem. Int. Ed.* **2014**, *53*, 52–56.
39. Supansomboon, S.; Porkovich, A.; Dowd, A.; Arnold, M.D.; Cortie, M.B. Effect of precursor stoichiometry on the morphology of nanoporous platinum sponges *ACS Appl. Mater. Interfaces* **2014**, *6*, 9411–9417.
40. Cortie, M.B. Simulation of metal solidification using a cellular automaton. *Metall. Trans. B* **1993**, *24*, 1045–1053.
41. Cortie, M.B.; Maaroof, A.I.; Stokes, N.; Mortari, A. Mesoporous gold sponge. *Aust. J. Chem.* **2007**, *60*, 524–527.
42. Cole, K.J.; Carley, A.F.; Crudace, M.J.; Clarke, M.; Taylor, S.H.; Hutchings, G.J. Copper manganese oxide catalysts modified by gold deposition: The influence on activity for ambient temperature carbon monoxide oxidation. *Catal. Lett.* **2010**, *138*, 143–147.
43. Epling, W.S.; Hoflund, G.B.; Weaver, J.F.; Tsubota, S.; Haruta, M. Surface characterization study of Au/a-Fe_2O_3 and Au/Co_3O_4 low-temperature CO oxidation catalysts. *J. Phys. Chem.* **1996**, *100*, 9929–9934.
44. Vitos, L.; Ruban, A.V.; Skriver, H.L.; Kollar, J. The surface energy of metals. *Surf. Sci.* **1998**, *411*, 186–202.
45. Wang, X.; Frenzel, J.; Wang, W.; Ji, H.; Qi, Z.; Zhang, Z.; Eggeler, G. Length-scale modulated and electrocatalytic activity enhanced nanoporous gold by doping. *J. Phys. Chem. C* **2011**, *115*, 4456–4465.
46. Maaroof, A.I.; Cortie, M.B.; Smith, G.B. Optical properties of mesoporous gold films. *J. Opt. A Pure Appl. Opt.* **2005**, *7*, 303–309.